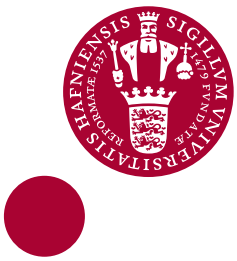

Remote sensing of vegetation dynamics in drylands

Evaluating vegetation optical depth (VOD) using AVHRR NDVI and in situ green biomass data over West African Sahel

Tian, Feng; Brandt, Martin Stefan; Liu, Yi Y.; Verger, Aleixandre; Tagesson, Håkan Torbern; Diouf, Abdoul A.; Rasmussen, Kjeld; Mbow, Cheikh; Wang, Yunjia; Fensholt, Rasmus

Published in:
Remote Sensing of Environment

DOI:
10.1016/j.rse.2016.02.056

Publication date:
2016

Document version
Peer reviewed version

Remote sensing of vegetation dynamics in drylands: Evaluating vegetation optical depth (VOD) using AVHRR NDVI and *in situ* green biomass data over West African Sahel

Feng Tian [a, b], Martin Brandt [a], Yi Y. Liu [c], Torbern Tagesson [a], Aleixandre Verger [d], Kjeld Rasmussen [a], Abdoul A. Diouf [e], Cheikh Mbow [f], Yunjia Wang [b], Rasmus Fensholt [a]

[a] Department of Geosciences and Natural Resource Management, University of Copenhagen, 1350 Copenhagen, Denmark

[b] School of Environment Science and Spatial Informatics, China University of Mining and Technology, 221116 Xuzhou, China

[c] ARC Centre of Excellence for Climate Systems Science & Climate Change Research Centre, University of New South Wales, Sydney, 2052 New South Wales, Australia

[d] CREAF, Cerdanyola del Vallès, 08193 Catalonia, Spain

[e] Centre de Suivi Ecologique (CSE), BP 15532 Dakar-Fann, Senegal

[f] Science Domain 6, ICRAF (World Agroforestry Center), 00100 Nairobi, Kenya

Abstract

Monitoring long-term biomass dynamics in drylands is of great importance for many environmental applications including land degradation and global carbon cycle modeling. Biomass has extensively been estimated based on the normalized difference vegetation index (NDVI) as a measure of the vegetation greenness. The vegetation optical depth (VOD) derived from satellite passive microwave observations is sensitive to the water content in total aboveground vegetation layer and minimally affected by atmospheric conditions. VOD therefore provides a complementary data source to NDVI for monitoring biomass dynamics in drylands, yet further evaluations based on ground measurements are needed for an improved understanding of the potential advantages. In this study, we assess the capability of a long-term VOD dataset (1992–2011) to capture the temporal and spatial variability of *in situ* measured green biomass (woody foliage and herbaceous masses) in the semi-arid Senegalese Sahel. Results show that the magnitude and peaking time of VOD are highly correlated with woody foliage mass whereas NDVI seasonality is primarily governed by the green herbaceous vegetation layer in the study area. Moreover, VOD is found to be robust against typical NDVI drawbacks of saturation effect as well as dependence on plant structure (woody and herbaceous vegetation compositions) and species compositions when used as a proxy for vegetation productivity. Finally, both VOD and NDVI well reflect the spatial and inter-annual dynamics of the *in situ* green biomass data; however, the seasonal metrics leading to the best correlations differ between them. While the observations in October (period of *in situ* data collection) perform best for VOD ($r^2 = 0.88$), the small growing season integral (sensitive to recurrent vegetation) have the highest correlations for NDVI ($r^2 = 0.90$). Overall, in spite of the coarse resolution, the study shows that VOD is an efficient proxy for estimating green biomass of the entire vegetation stratum in the semi-arid Sahel and likely also in other dryland areas.

Keywords: Biomass, VOD, satellite passive microwave, woody cover, plant structure, vegetation species compositions, saturation effect, semi-arid Sahel

1. Introduction

Improved understanding of changes in dryland biomass is relevant to the understanding of the global carbon balance given that approximately 41% of the Earth's terrestrial surface is covered by drylands (Adeel et al. 2005). Recent studies showed that dryland biomass is a more dominant driver for global carbon cycle inter-annual variability as compared to the tropical rainforests (Ahlstrom et al. 2015; Poulter et al. 2014). The understanding of the spatial distribution and temporal trends in vegetation cover, biomass and productivity in drylands is central to many research disciplines.

Optical remote sensing provides a unique way of achieving full coverage of global drylands and have facilitated monitoring of biomass dynamics since the early 1980s, using the normalized difference vegetation index (NDVI), derived from the red and near-infrared reflectance bands of the NOAA (National Oceanic and Atmospheric Administration) AVHRR (Advanced Very High Resolution Radiometer) sensors. As a measurement of chlorophyll abundance and energy absorption (Myneni and Hall 1995; Tucker and Sellers 1986), NDVI has been widely used as a proxy for vegetation productivity (e.g. Myneni et al. (1997) and Nemani et al. (2003)). However, several well-known limitations of NDVI for robust estimation of biomass in drylands exist. NDVI is sensitive to the green components and insensitive to woody components where the majority of carbon stores (Tucker 1979). Also, above ground vegetation production is not always linked to greenness in a uniform way and the plant structure (woody and herbaceous vegetation compositions) and vegetation species compositions have been shown to impact the biomass-NDVI relationship (Goetz et al. 1999; Mbow et al. 2013; Prince and Goward 1995; Wessels et al. 2006). Moreover, atmospheric effects (e.g. water vapor, clouds and aerosols) contaminate images retrieved from the red and near-infrared bands in general and from the spectrally wide AVHRR bands in particular (Holben 1986). This is not only inherent to tropical moist regions but also a problem in semi-arid areas like the African Sahel characterized by a distinctive growing season, where prevailing cloud cover is often obscuring regular monitoring of vegetation resources (Fensholt et al. 2011; Fensholt et al. 2007). Also, optical remote sensing during the dry season can be strongly influenced by atmospheric dust (e.g. the cold-dry and dusty trade wind known as the Harmattan) causing a noisy NDVI signal (Achard and Blasco 1990; Ahearn and de Rooy 1996). Finally, a well-known factor reducing the capability of

NDVI to estimate biomass is the saturation effect due to the strong absorption in the red wavelength (Sellers 1985). With an increasing amount of green vegetation, the sensitivity of NDVI is reduced and BOA (bottom of atmosphere) reaches a saturation point (Gitelson et al. 1996) at approximately 0.8 units (dependent on the specific response function of the satellite sensor). Despite the lower amount of biomass present in dryland areas, NDVI saturation effects have also been reported to impact vegetation monitoring (Fensholt 2004; Milich and Weiss 2000; Olsson et al. 2005).

Several previous studies have investigated vegetation dynamics based on satellite passive microwave observations (Becker and Choudhury 1988; Choudhury and Tucker 1987; Choudhury et al. 1987; Jones et al. 2014; Jones et al. 2011; Min and Lin 2006; Njoku and Chan 2006; Owe et al. 2001; Qian et al. 2015; Shi et al. 2008). Unlike the optical remote sensing based VI (sensitive to greenness), the vegetation information retrieved from satellite passive microwave observations (here referred as vegetation optical depth, VOD) is sensitive to the water content in the total aboveground vegetation, including both green (e.g. woody foliage and herbaceous) and non-green components (e.g. tree stems and branches) (Shi et al. 2008). For a given area of canopy cover, woody and herbaceous vegetation may show similar greenness levels whereas hold different levels of water content due to the different plant structures. Also, the seasonal variation of water content in woody and herbaceous vegetation would be distinct from each other dependent on the specific vegetation species. Hence, VOD may be a more robust proxy for the total vegetation biomass as compared to NDVI (Jones et al. 2013). Furthermore, due to the longer wavelength and stronger penetration capacity of microwave, VOD is insensitive to atmosphere and cloud contamination effects and can therefore provide valid global observations at almost daily frequency, of benefit to land surface phenology monitoring (Jones et al. 2012). Moreover, VOD has less saturation effect than NDVI (Jones et al. 2011). These features all together make VOD a promising proxy for biomass at regional to global scales, despite the coarse spatial resolution of historical data (> 10 km) as a result of the low energy of the natural microwave emissions from the Earth's surface.

Recently, a long-term VOD dataset covering more than 20 years was generated by combining observations from a series of passive microwave instruments (Liu et al. 2011a; Liu et al. 2015). This unique dataset provides new opportunities to gain insights of global vegetation changes from the microwave region of the spectrum over

a period almost comparable with AVHRR sensors. Based on this VOD dataset, long-term changes in global drylands have been investigated and, as expected, it is found that the inter-annual variations of VOD are mainly driven by precipitation (Andela et al. 2013; Liu et al. 2013a; Liu et al. 2013b). However, to the authors' best knowledge no analysis including *in situ* biomass measurements has been conducted to examine the spatial and temporal dynamics of VOD data in relation to different compositions of woody and herbaceous vegetation. Moreover, the annual sum/maximum and the growing season integral of NDVI have a proven record of showing realistic estimations for biomass accumulation in drylands (Diouf et al. 2015; Meroni et al. 2014; Prince 1991; Tucker et al. 1983; Wessels et al. 2006). However, whether these seasonal metrics apply in the same way for VOD data has not been assessed yet.

In this study, our overall objective is to gain an improved understanding of the performance of VOD data for monitoring long-term vegetation dynamics in dryland areas, by comparing with the well-known NDVI based approach and *in situ* measurements of green biomass (woody foliage and herbaceous masses)in the semi-arid Senegalese Sahel during the period 1992–2011. Firstly, we explore the VOD responses to different woody and herbaceous vegetation compositions in the study area characterized by a pronounced north-south gradient in woody cover and green biomass. Then, we assess the performance of different VOD metrics for their capability to reflect green biomass dynamics in both spatial and temporal domains.

2. Data

2.1. Study area

All *in situ* sites are located in the semi-arid Sahel zone of Senegal (Fig. 1). The Sahel can be separated into three zones, following a rainfall gradient from the northern Sahel (150–300 mm annual rainfall), over the central Sahel (300–500 mm) to the southern Sahel (500–700 mm). Driven by the rainfall, the vegetation density also shows a clear north–south increasing gradient with mean annual green biomass varying from approximately 1000 kg DM (dry matter) ha^{-1} at the northern sites to >4500 kg DM ha^{-1} at the southern sites (calculated from data described in section 2.4.2). The entire region is characterized by savannas consisting of herbaceous and

117 woody trees and shrubs. The herbaceous layer is dominated by annual plants growing from late June to early
118 October, however strongly dependent on annual rainfall distribution (de Ridder et al. 1982; Rietkerk et al. 1996).
119 The phenological behavior of woody plants is mainly evergreen, semi-evergreen or deciduous (Le Houérou
120 1980), showing distinct different phenological cycles as compared to the herbaceous layer present only during
121 the rainy season. The mean woody cover map during 2000–2013 produced by Brandt et al. (2016) at 1 km
122 spatial resolution was used to indicate the spatial variation of plant structure in the study area, with a woody
123 cover increases from < 3% in the north to > 40% in the south . Whereas herbaceous dominates the green biomass
124 in the north, the woody foliage produces higher biomass than the herbaceous in the south (Diouf et al. 2015).

125

126

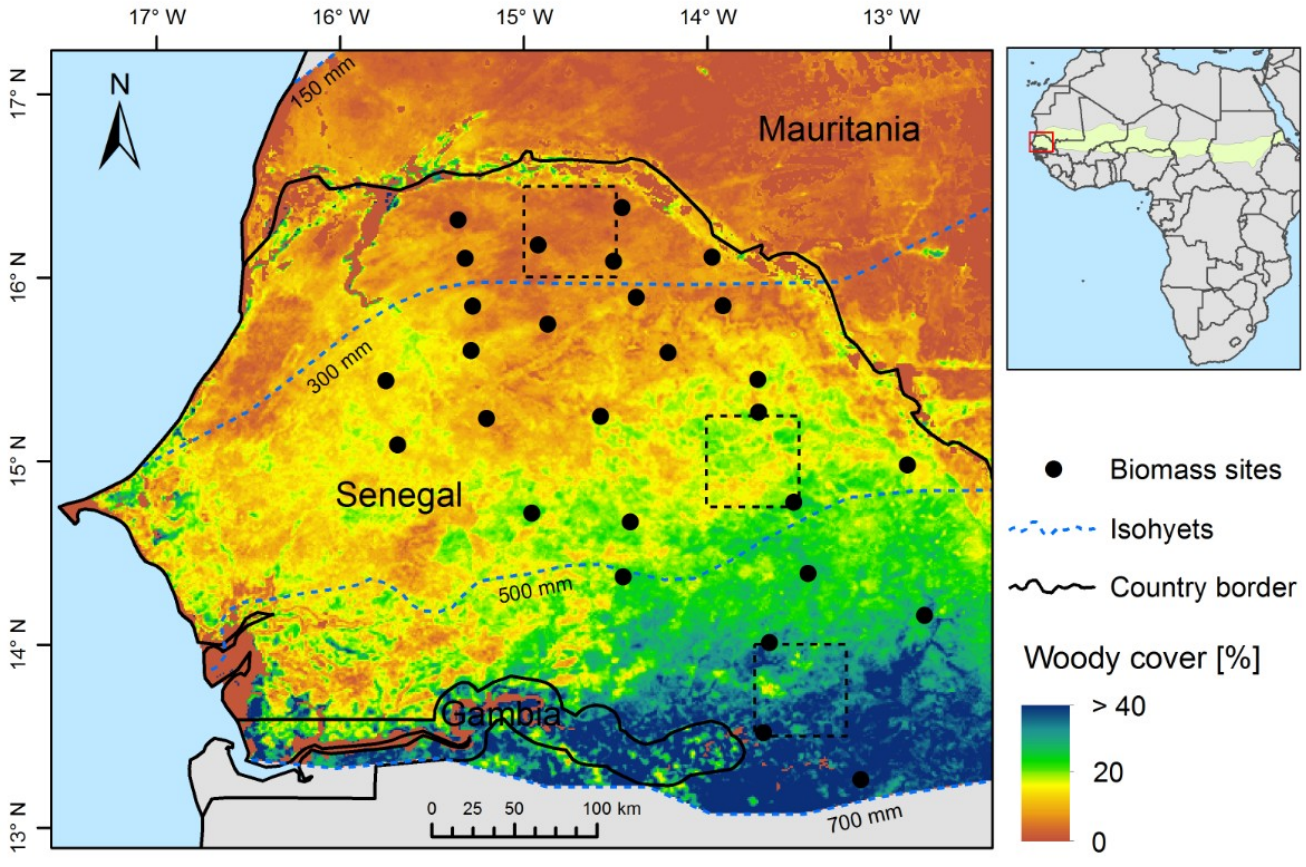

127

Fig. 1. Location of *in situ* observation sites in Senegal with a background showing mean woody cover during 2000–2013 (Brandt et al. 2016). The areas indicated by the dashed black boxes are further analyzed in Fig. 4A. The Sahel region and the Senegalese study area are highlighted in the map of Africa (top right).

2.2. VOD data

The VOD dataset used is derived from observations of a series of passive microwave instruments onboard different satellites, including the Special Sensor Microwave Imager (SSM/I) of the Defense Meteorological Satellite Program, the Advanced Microwave Scanning Radiometer – Earth Observing System (AMSR-E) onboard the Aqua satellite, and the radiometer of the WindSat (Liu et al. 2015). Briefly, the satellite based passive microwave observations (brightness temperature, T_b) consist of three components: 1) the radiation from the soil layer attenuated by the overlaying vegetation, 2) the upward radiation from the vegetation, and 3) the downward radiation from the vegetation, reflected upward by the soil layer and again attenuated by the vegetation (Mo et al. 1982) as shown in the equation 1.

$$T_b^P = T_{S_{e_r}}^P \Gamma^P + (1-\omega^P)T_C(1-\Gamma^P) + (1-e_r^P)(1-\omega^P)T_C(1-\Gamma^P)\Gamma^P \quad (1)$$

where P is the polarization (horizontal and vertical); T_S and T_C are the thermometric temperatures of the soil and the canopy, respectively; e_r is the soil emissivity determined by soil moisture, temperature and roughness; ω is the single scattering albedo; Γ is the vegetation transmissivity determined by VOD (τ, dimensionless) and observing incidence angle (μ) in the equation 2.

$$\Gamma = exp(-\tau/cos\,\mu) \quad (2)$$

The VOD is a function of the vegetation dielectric properties, responding primarily to the water content in total aboveground biomass including green and non-green components, varying with the vegetation geometric structure and the sensor wavelength and viewing angle (Jackson and Schmugge 1991).

The Land Parameter Retrieval Model (LPRM) retrieval algorithm (Meesters et al. 2005; Owe et al. 2008; Owe et al. 2001), developed from the above radiative transfer model, can derive soil moisture and VOD

simultaneously by assuming that VOD was polarization independent especially for randomly distributed crops and natural vegetation at satellite scales and that temperatures of the soil surface and canopy were equal during night-time. LPRM can be applied to observations from different satellites with varying microwave wavelengths and viewing angles. Accordingly, VOD datasets were derived from observations from SSM/I, AMSR-E and WindSat (Liu et al. 2015). Due to the dependence of sensor characteristics, VOD values vary between these three instruments. However, these three sensors have reasonably long overlapping periods, and their temporal dynamics are highly correlated for most of the Earth's land surface and in drylands in particular. The cumulative distribution function (CDF) matching approach was therefore conducted to merge these three VOD datasets into one long term time series over 1992-2011 (Liu et al. 2011a; Liu et al. 2011b).

In the merged VOD dataset, SSM/I observation is used from January 1992 through June 2002 before the AMSR-E started operating, while AMSR-E is used from July 2002 through September 2011. WindSat observation is used after AMSR-E stopped collecting data in early October 2011. The temporal consistency of this merged dataset was examined using both global and humidity zone averaged VOD anomaly series (similar to the method applied by Tian et al. (2015)) and found no artifacts in the time series to coincide with sensor shifts (see supplementary materials Fig. S1). The VOD value ranges from 0 to roughly 1.3 in the merged VOD dataset, and it is aggregated to 0.25 degree (~25 km) spatial resolution and monthly intervals.

2.3. GIMMS3g AVHRR NDVI

Although the GIMMS (Global Inventory Modeling and Mapping Studies) NDVI product is not free from problems (Horion et al. 2014; Tian et al. 2015), it has been reported to be the most suitable for long-term vegetation analysis amongst several available long-term AVHRR NDVI datasets (Beck et al. 2011; Tian et al. 2015) and trend analysis of the GIMMS NDVI products have been shown to be in agreement with trends from MODIS (Moderate Resolution Imaging Spectroradiometer) NDVI products particularly in drylands (Fensholt and Proud 2012; Fensholt et al. 2009). The latest version of the GIMMS AVHRR NDVI data (GIMMS3g) was therefore used in this study and includes the following overall pre-processing steps (for a detailed description refer to Pinzon and Tucker (2014)): The AVHRR channel 1 (visible band) and channel 2 (near-infrared band) are calibrated by applying time-varying vicarious calibrations methods (Cao et al. 2008; Los 1998; Vermote and

177 Kaufman 1995; Wu et al. 2010). The varying solar zenith angle effects on NDVI values (caused by orbital drift)
178 are reduced using an adaptive empirical mode decomposition/reconstruction procedure (Pinzon et al. 2005). The
179 AVHRR/2 and AVHRR/3 NDVI probability density functions were calibrated by applying a Bayesian analysis
180 using the SeaWiFS (Sea-Viewing Wide Field-of-view Sensor) NDVI data as prior information (Pinzon and
181 Tucker 2014). Maximum value compositing over 15 days was applied to reduce the atmospheric effects.
182 Furthermore, stratospheric aerosol correction was applied during the El Chichon (April 1982–December 1984)
183 and Mt Pinatubo (June 1991–December 1993) volcanic stratospheric aerosol periods (Tucker et al. 2005). The
184 GIMMS3g NDVI dataset provides two images per month with a spatial resolution of 1/12°. We averaged the
185 two NDVI values in each month during 1992–2011 for consistency with the VOD dataset whereas the original
186 spatial resolution of data was kept.

187 ***2.4. In situ measurements***

188 Annual biomass data was collected by the Centre de Suivi Ecologique (CSE) in Senegal from 1992 to 2011
189 (except for 2004). The measurements were conducted at the end of the growing season (October) and the data
190 has shown to be consistent with satellite time series (Brandt et al. 2015b). Biomass of herbaceous and woody
191 foliage layers were measured separately and summed to obtain the total biomass in kg DM ha^{-1}.

192 • The herbaceous collection followed the original method proposed by the International Livestock Centre for
193 Africa (ILCA) (Diouf et al. 1998) based on stratification of the herbaceous layer into four strata (bare soil
194 patches and low, medium and high herbaceous bulk density). At each field site, a 1 km transect was selected,
195 along which 35–100 plots of one square meter were randomly placed, considering the vegetation
196 stratification. For each of the strata, all fresh vegetation collected was weighed and three 200 g samples of
197 each stratum were dried in an oven to obtain the dry matter to wet weight ratio. The dry matter weight of
198 each stratum is obtained by multiplying the mean wet weight by the dry matter ratio. Then, the site
199 herbaceous mass is calculated by weighting the mean mass of each stratum by the relative frequency of the
200 stratum along the transect.
201 • Foliage biomass measurements of trees and shrubs were performed for each site in two steps: 1) every two
202 years, all species were sampled within four circular plots (of 1/16 to 1 ha) placed every 200 m along the

selected transect. Along with other parameters, the circumferences of alive trunks were measured for calculation of the potential woody foliage biomass using the allometric relationships established for Sahelian tree and shrub species (Cissé 1980; Diallo et al. 1991; Diouf and Lambin 2001; Hiernaux 1980). 2) These potential values were then adjusted to each particular year and site conditions with leaf samples of 10 branch lets from each of the most representative species. Then, the total woody foliage biomass of each site was obtained by summing up all the investigated woody species.

A detailed description of the method is given in Diouf et al. (2015). We examined the VOD pixels covering each site with Google Earth and excluded 5 highly heterogeneous plots that are located either close to rivers or mixed cropping and forest areas (whereas the measurements were taken in the forest area only), leaving 27 relatively homogeneous sites (shown in Fig. 1) with 516 measurements for further analysis (not all sites were surveyed by CSE each year).

2.5. Rainfall data

The ARC2 (African Rainfall Climatology version 2) daily rainfall data (0.1° spatial resolution) (Novella and Thiaw 2013) were used in the study. For consistency with the VOD dataset, we summed the daily rainfall values in each month during 1992–2011 whereas the original spatial resolution of data was kept.

3. Methods

3.1. Comparing VOD and NDVI responses to woody and herbaceous vegetation compositions

To understand the VOD responses to woody and herbaceous vegetation compositions, we compared its spatial patterns and seasonal variations to NDVI over the study area characterized by a clear north-south vegetation gradient. The pixel-wise monthly VOD, NDVI and ARC2 rainfall means across the entire period (1992–2011) were calculated for the study area, respectively. In order to better illustrate the differences between VOD and NDVI, we further examined the seasonal patterns of three sub regions (Fig. 1) along the north-south gradient (with mean woody cover of 3%, 15% and 34%, respectively). The phenological behavior (i.e. the

temporal distribution of green biomass) of herbaceous and dominant woody species in the study area (evergreen, semi-evergreen and deciduous), produced by Mougin et al. (1995), Mougin et al. (2014) and (Brandt et al. 2016), were used to assist interpretation of the VOD seasonal variations. Moreover, we compared the relationships between annual maximum VOD/NDVI (calculated from the long-term monthly mean during 1992–2011) and woody cover over the study area. In this context, the woody cover data was averaged to the VOD spatial resolution while the median of NDVI pixels overlapping the VOD pixel was used.

3.2. Evaluating VOD and NDVI metrics for reflecting green biomass dynamics

3.2.1. Seasonal metrics

The annual maximum, annual sum, growing season large integral (integration of NDVI values during the growing season) and small integral (integration of NDVI amplitudes during the growing season) (Fig. 2) have been widely used to estimate biomass productivity/accumulation with NDVI time series observations based on linear regression (de Jong et al. 2011; Fensholt et al. 2015; Tian et al. 2013). Here, we tested the performance of these metrics for VOD data against the annual *in situ* green biomass data at 27 sites over 20 years using ordinary least square linear regressions. As the *in situ* green biomass data were collected during month of October, we also examined the performance of October VOD observations. For comparison purposes, NDVI data was also analyzed against the *in situ* green biomass data. The growing season integrals were calculated using the TIMESAT software (Jonsson and Eklundh 2002, 2004). The start of season was set to 20% of the amplitude for both VOD and NDVI data. To be in line with the time of *in situ* data collection, the end of season was set to 80% of the amplitude for the VOD data and 50% for the NDVI data (different thresholds applied due to the later drop of VOD values as compared to NDVI as shown in Fig. 2).

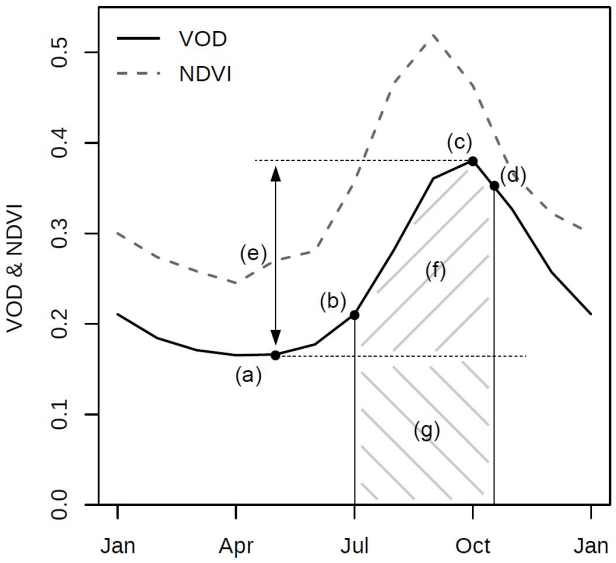

247

248 **Fig. 2.** Illustration of the seasonal vegetation metrics used in this study: (a) annual minimum, (b) start of season, (c) annual
249 maximum, (d) end of season, (e) amplitude, (f) small integral, and (f)+(g) large integral. The VOD and NDVI curves are the
250 mean of the entire study area (as shown in Fig. 1) during 1992–2011.

251 3.2.2. Data comparison

252 The comparisons between VOD/NDVI metrics and *in situ green* biomass data were performed in two steps.
253 In the first step, we assessed the performance of VOD and NDVI metrics for reflecting green biomass dynamics
254 at pixel level across a gradient of increasing biomass from north to south of the study area. For each year during
255 1992–2011, we calculated all the VOD and NDVI seasonal metrics for each pixel overlapping the *in situ* sites.
256 Then, each of the seasonal metrics was regressed against the corresponding biomass data for the sites located in
257 the northern, central, southern and entire study area, respectively. In the second step, we focused on the
258 capabilities of VOD and NDVI metrics for reflecting green biomass inter-annual dynamics over all *in situ* sites.
259 Due to differences in the spatial resolution (VOD 25 km, NDVI 8 km, and biomass data 1 km), the heterogeneity
260 effect inevitably introduces bias between *in situ* measurements and remote sensing observations, impeding a
261 successful evaluation of the temporal dynamics of the VOD and NDVI data. To reduce this bias and to highlight
262 the aspects of temporal dynamics, we therefore averaged all the available *in situ* data over the entire study area
263 for each year and the corresponding pixel-scale VOD/NDVI metrics calculated in the first step, respectively.
264 This averaging method has been widely applied for evaluating satellite observations using *in situ* measurements

265 (Dardel et al. 2014; Jackson et al. 2010; Tagesson et al. 2013; Zeng et al. 2015). The coefficient of determination
266 (r^2) of Pearson product-moment correlation and root mean square error (RMSE) were calculated for each pair of
267 comparison in both steps.

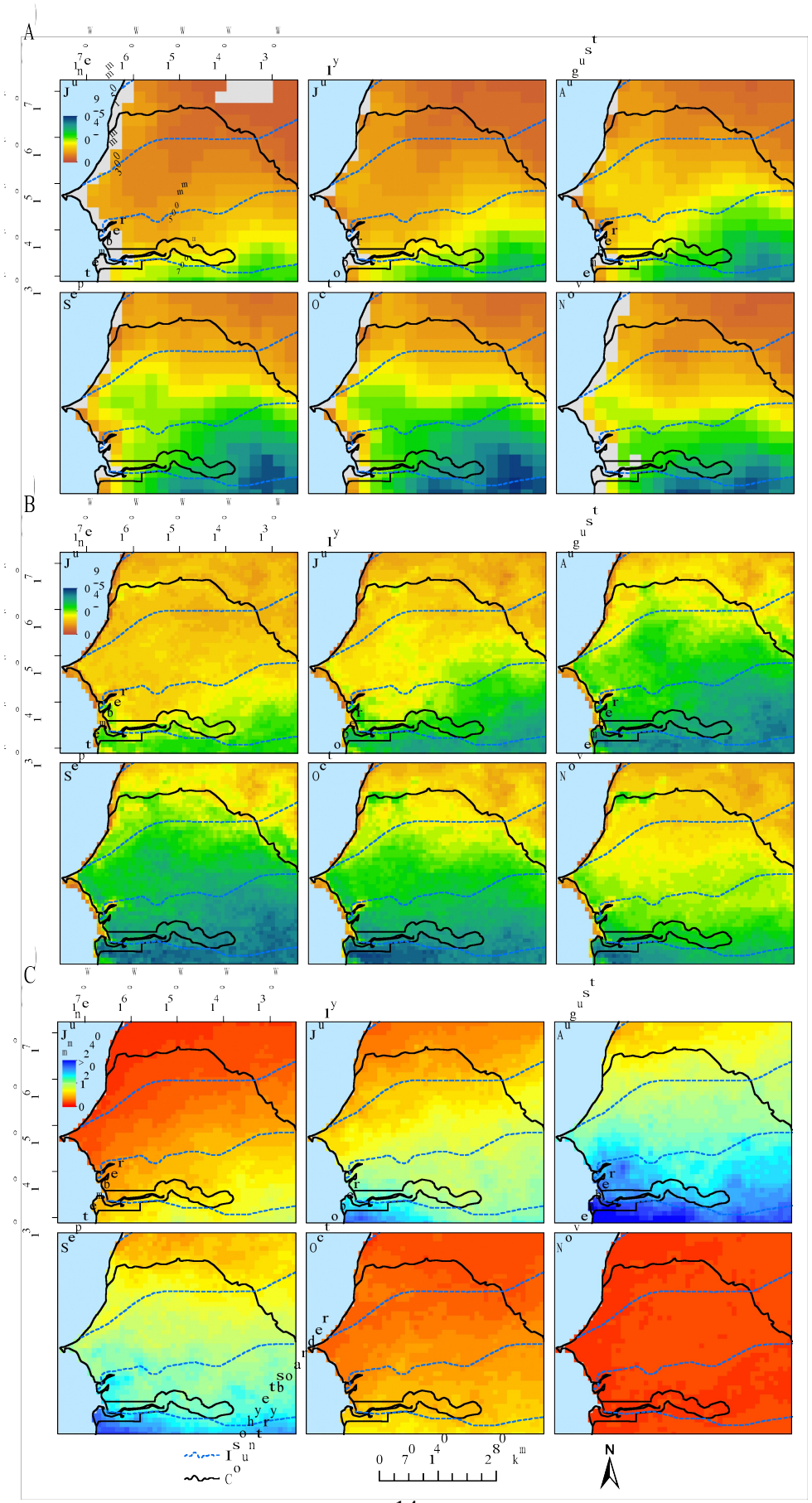
A
B
C
N

Fig. 3. Spatial patterns of monthly mean VOD (A), NDVI (B) and annual rainfall (mm) (C) during 1992–2011 from June to November.

4. Results

4.1. VOD responses to woody and herbaceous vegetation compositions

The spatial patterns of VOD, NDVI and rainfall in the study area are shown for the months covering the rainy season (June-November) (Fig. 3). Despite the coarse spatial resolution of the VOD data, a clear north-south gradient is observed in a similar way to the spatial patterns of NDVI. The seasonal patterns over the course of the year of the selected sub regions (dashed black boxes in Fig. 1) are shown in Fig. 4A. VOD starts to increase simultaneously with NDVI for all sub regions in the study area, in line with the onset of the rainfall. During the growth phase, NDVI shows identical temporal development from north to south, reaching the second highest value in August, peaking in September and then decreasing in October to a lower level followed by a further drop in November. VOD data however, show high values in both September and October from north to south, with peaking time changing from September in the north to October in the south. The delay in VOD peak time from north to south corresponds to the longitudinal gradient of woody cover (Fig. 1) with average values of 3%, 15% and 34% for the northern, central and southern sub regions, respectively. This positive shift in the date of the peak in VOD can be partly explained by the higher contribution of woody foliage (see the woody foliage and herbaceous biomass of each sub region in Fig. 4A) which are characterized by longer growing seasons and later seasonal peaking than the herbaceous layer (Fig. 4B). The higher sensitivity of VOD than NDVI to woody vegetation is also indicated by their relationships with woody cover (Fig. 4C). With increasing woody cover, VOD increases linearly while NDVI saturated around 20% of woody cover. Another noticeable point is that in areas with a woody cover less than ~8% the VOD values shows less variation (standard deviation equals 0.04) than NDVI values (standard deviation equals 0.06).

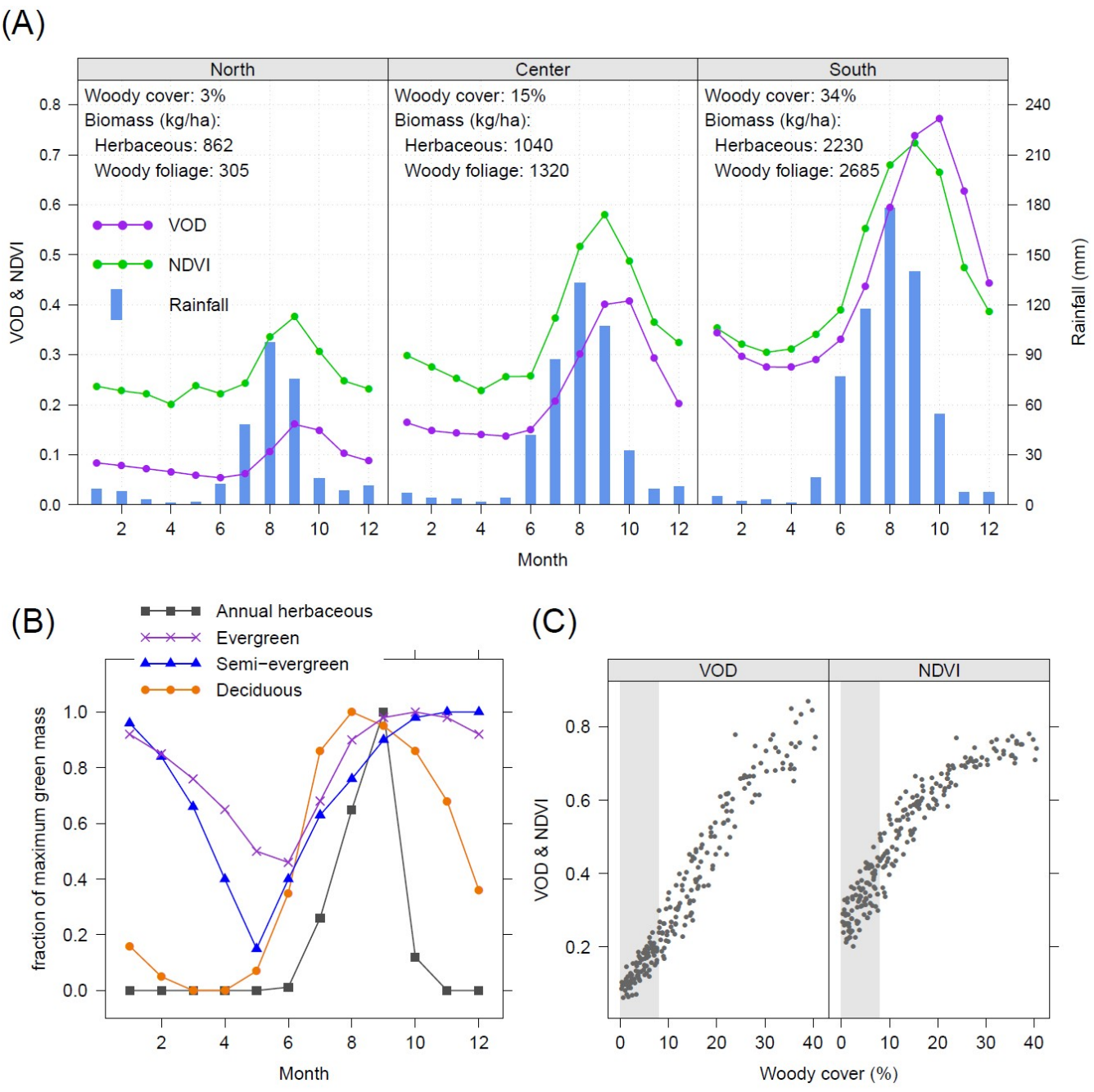

Fig. 4. (A) Seasonal patterns of mean VOD, NDVI and rainfall during 1992–2011 in the sub regions of northern, central and southern parts of the study area (average of all pixels in each of the dashed black boxes in Fig. 1). The biomass of herbaceous and woody foliage is given by averaging the *in situ* sites within each selected area. (B) Phenology of typical Sahelian woody and herbaceous vegetation (expressed as fraction of maximum green mass, extracted from Mougin et al. (1995), Mougin et al. (2014) and Brandt et al. (2016)). Although variations can be observed from north to south, the general behavior follows these curves. (C) Spatial relationships of woody cover and the annual maximum VOD/NDVI calculated

299 from the monthly mean during 1992–2011 over the study area. The pixels with woody cover less than 8% are high
300 lightened in a grey background.

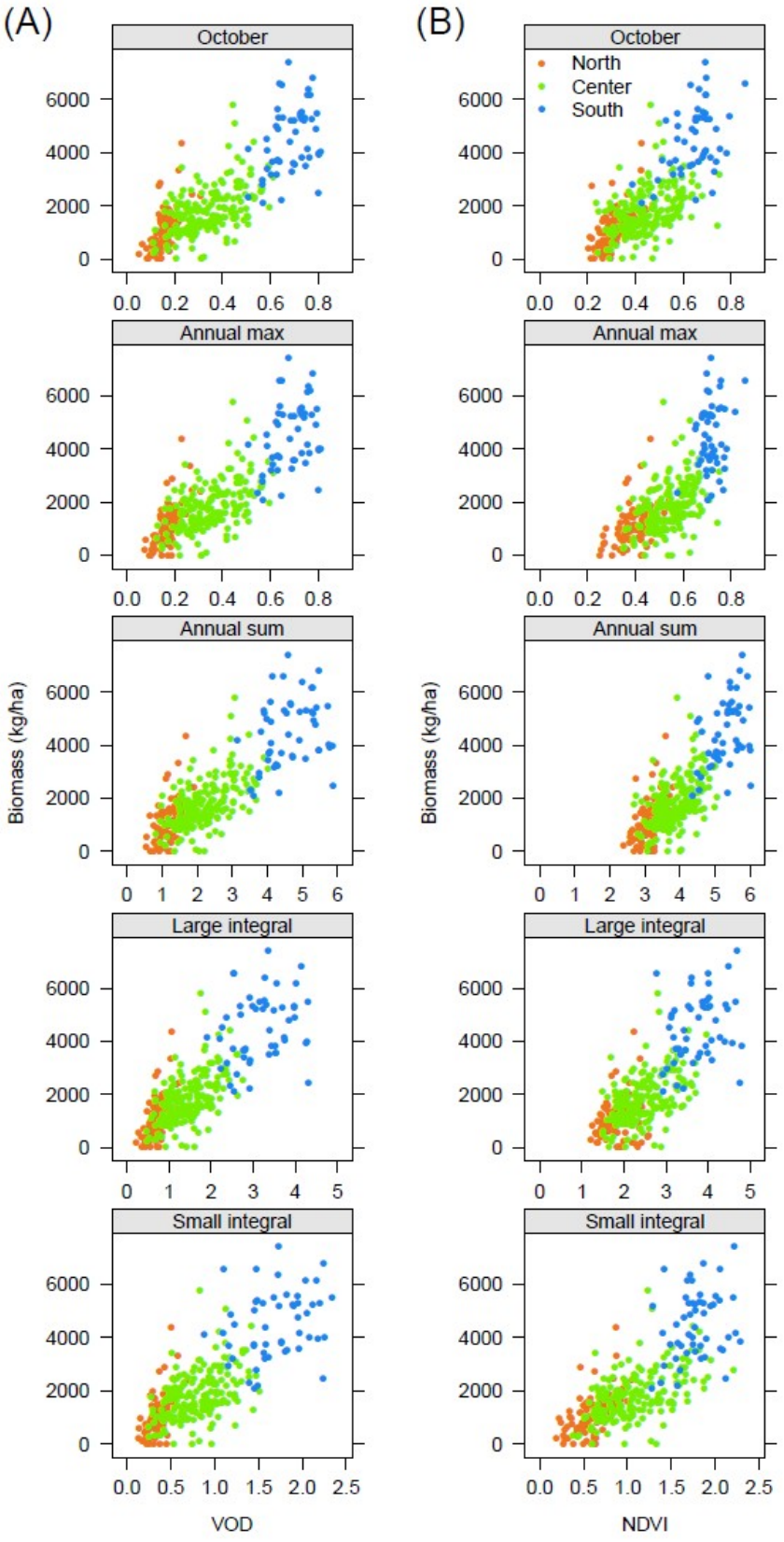
(A)
(B)
October
Annual max
Annual sum
Large integral
Small integral
North
Center
South
Biomass (kg/ha)
VOD
NDVI

301

Fig. 5. Scatter plots between *in situ* green biomass data collected at the end of growing season (October) and seasonal metrics ((A) VOD and (B) NDVI) of October, annual max, annual sum, large integral and small integral.

Table 1. r^2 values between different VOD/NDVI metrics and *in situ* green biomass measurements of the sites located in the northern, central, southern and entire study area (corresponding with the scatter plots in Fig. 5). The number of observations is given as "N". Note that "^" and "*" mean the linear correlation is significant at 0.01 and 0.05 levels, respectively.

Metrics	VOD								NDVI							
	North N=91		Centre N=192		South N=52		All N=334		North N=91		Centre N=192		South N=52		All N=334	
	r^2	RMSE	r^2	RMSE	r^2	RMSE	r^2	RMSE	r^2	RMSE	r^2	RMSE	r^2	RMSE	r^2	RMSE
October	0.38^	588	0.30^	755	0.12*	1177	0.64^	854	0.31^	621	0.21^	805	0.21^	1121	0.55^	964
Annual max	0.42^	568	0.30^	758	0.12*	1182	0.65^	852	0.20^	671	0.19^	816	0.05	1229	0.52^	997
Annual sum	0.27^	641	0.35^	728	0.07	1216	0.66^	836	0.23^	656	0.23^	794	0.16^	1156	0.61^	895
Large integral	0.37^	594	0.32^	745	0.06	1221	0.64^	854	0.07*	723	0.26^	778	0.08*	1207	0.56^	950
Small integral	0.33^	614	0.21^	806	0.06	1219	0.59^	916	0.33^	613	0.28^	766	0.06	1217	0.56^	947

4.2. Performance of VOD and NDVI metrics for reflecting green biomass dynamics

The scatter plots between pixel-scale VOD/NDVI metrics and plot-scale *in situ* green biomass data are shown in Fig. 5 and the r^2 and RMSE values are summarized in Table 1. The statistical results for the averaged VOD/NDVI metrics and *in situ* green biomass data are summarized in Table 2 and Fig. 6 shows the best and poorest metrics for VOD and NDVI, respectively, in relation to the temporal changes of *in situ* data. These results are interpreted from two aspects: 1) the performance of VOD and NDVI metrics across a gradient of increasing biomass, and 2) the performance of VOD and NDVI metrics for reflecting inter-annual green biomass dynamics over all the *in situ* sites.

1) In line with the rainfall and woody cover, the green biomass is also characterized by an increasing gradient from north to south of the study area. Like the relationship with woody cover in Fig. 4C, the NDVI maximum shows clear saturation effect in the southern part while VOD maximum does not (Fig. 5). Taking all sites into account, all of the seasonal metrics show significant ($p < 0.01$) correlations with the green biomass data and the r^2 values (0.59 – 0.66 for VOD and 0.52 – 0.61 for NDVI) are higher as

compared to those for individual parts of the study area (Table 1). With a large amount of observations in the central part (N = 192), significant correlations ($p < 0.01$) are obtained between biomass data and all seasonal metrics (r^2 equals 0.21 – 0.35 for VOD and 0.19 – 0.28 for NDVI). In the northern part (N = 91), the seasonal metrics (except for NDVI large integral with $p < 0.05$ and $r^2 = 0.07$) also show significant correlations ($p < 0.01$) with the biomass data and the r^2 values (0.27 – 0.42 for VOD and 0.20 – 0.33 for NDVI) are comparable to those in the central part. The seasonal metrics show poorer performance (lower r^2 values, 0.06 – 0.12 for VOD and 0.05 – 0.21 for NDVI) in the southern part (N = 52) than in the northern and central parts, with many of them showing insignificant correlations ($p > 0.05$ for VOD annual sum, small and large integrals and NDVI annual max and small integral) with the biomass data. The VOD metrics outperform the NDVI counterparts in the northern, central and entire parts of the study area (except for the small integral in the central part). Whereas in the southern part, NDVI metrics of October, annual sum and large integral show better results than the VOD counterparts although both performs poorly in this part.

2) By averaging all the sites to reduce the bias caused by scale difference, all the VOD/NDVI metrics show improved correlation with the *in situ* green biomass data (Table 2) as compared to the pixel versus plot scale comparisons (Table 1). The metrics derived from both VOD and NDVI are able to reproduce the averaged *in situ* green biomass inter-annual dynamics at a similar level (Table 2 and Fig. 6). However, the metrics leading to the best correlations differ between the two indexes. The October VOD shows the best performance ($r^2 = 0.88$) among all of the VOD metrics, closely followed by the annual sum ($r^2 = 0.87$), annual max ($r^2 = 0.86$) and then the large integral ($r^2 = 0.83$) whereas the VOD small integral shows poorest performance ($r^2 = 0.64$) amongst all VOD and NDVI metrics. On the contrary, the NDVI small integral shows the best performance ($r^2 = 0.90$) while October NDVI shows the poorest ($r^2 = 0.68$). The NDVI large integral ($r^2 = 0.82$) shows a better performance than the NDVI annual sum ($r^2 = 0.72$) and annual max ($r^2 = 0.70$).

Table 2. Performance of different VOD and NDVI metrics for reflecting *in situ* green biomass inter-annual dynamics (1992–2011). All the available sites over the study area for each year were averaged to reduce the bias caused by scale difference. All of the r^2 obtained are significant at the 0.01 level.

Metrics	VOD		NDVI	
	r^2	RMSE	r^2	RMSE
October	0.88	175	0.68	283
Annual max	0.86	186	0.70	274
Annual sum	0.87	178	0.72	263
Large integral	0.83	204	0.82	209
Small integral	0.64	300	0.90	160

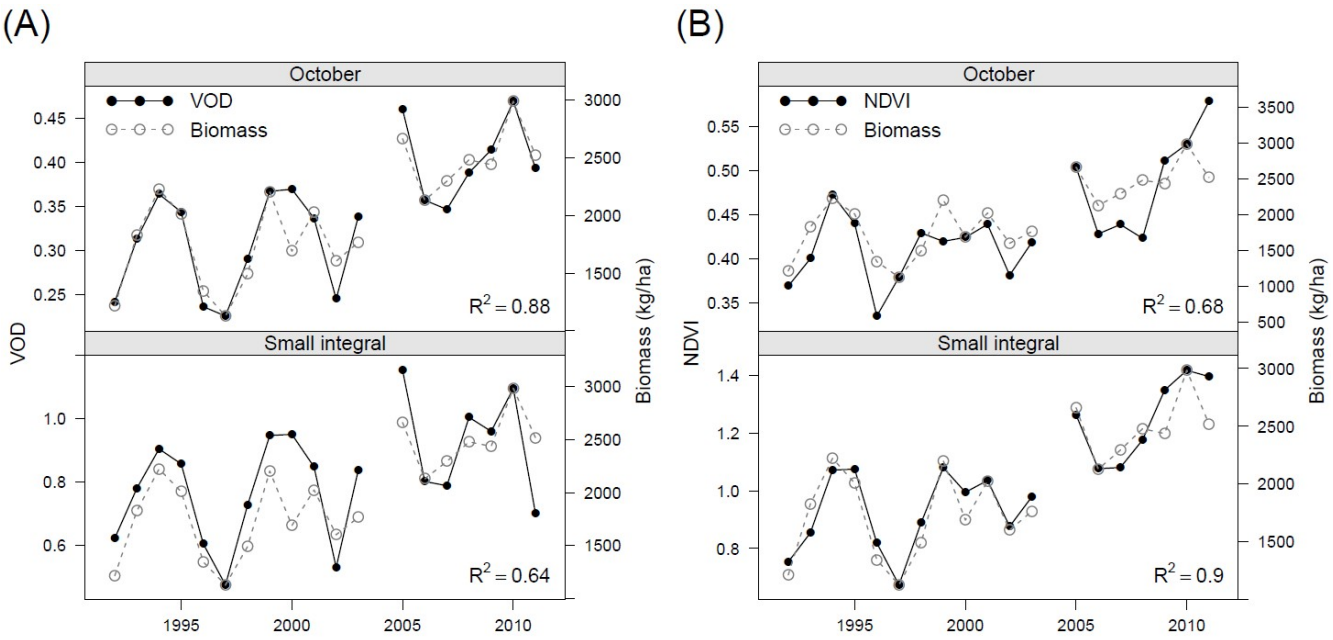

Fig. 6. Comparisons of the inter-annual dynamics between mean of all the *in situ* green biomass data collected at the end of growing season (October) and the corresponding (A) VOD and (B) NDVI metrics characterized by the highest and lowest r^2. The ranges of y axis at both sides are adjusted to match the years with minimum and maximum *in situ* green biomass (1997 and 2010, respectively) in each sub plot for improved visualization.

5. Discussion

NDVI is only sensitive to the greenness of the vegetation layer (woody foliage and herbaceous) whereas VOD is sensitive to water content from both the green and non-green (wood) parts. The *in situ* data collected at Dahra field site (supplementary material Fig. S2) shows that greenness and water content of the herbaceous layer are highly linked with each other particularly during the browning stage of the growing season, which is likely the same for woody foliage. Therefore, by comparing the seasonal patterns of VOD and NDVI (Fig. 4A) with the intra-annual dynamics of green biomass productivity (Fig. 4B), we can infer that the later peaking time of woody foliage (and likely the wood) as compared to herbaceous (expressed as the fraction of maximum green mass) result in the longer period of high VOD values (September and October) as compared to NDVI (peak in September). Consequently, VOD reflects the temporal development of woody vegetation more than NDVI, which was also shown by Jones et al. (2011) and Jones et al. (2013). Additionally, with less saturation effect, VOD also shows better performance than NDVI on quantifying the spatial variation of woody cover (Fig. 4C). Therefore, estimation of woody cover in global drylands is likely to benefit from this unique feature of VOD data. Specifically, there is a long-standing debate on the development of the woody cover of the Sahel. Available studies are limited to local scales, covering different periods and thus providing contradictory results that are not directly comparable: While some studies have reported decreases in woody cover (and thus presumably also in biomass) (Gonzalez et al. 2012) others have provided evidence for increases in woody cover (or related variables) (Brandt et al. 2015b; Hiernaux et al. 2009; Spiekermann et al. 2015). By calibration with existing woody cover maps (e.g. Brandt et al. (2016)), this VOD dataset could provide a spatially continuous estimation of woody cover changes since early 1990s.

Estimation of green biomass using the NDVI metrics has been reported to be influenced by varying woody and herbaceous vegetation compositions (Diouf et al. 2015; Wessels et al. 2006) as well as herbaceous species compositions (Mbow et al. 2013; Olsen et al. 2015), which is caused by the inconsistent relationship between greenness and biomass. Being uniformly responding to the water content in woody foliage and herbaceous (Fig. 4), VOD may be a more robust proxy for the green biomass. This is supported by the generally higher correlations between VOD metrics and *in situ* green biomass data as compared to NDVI metrics (Fig.5 and Table 1), even though VOD pixels have larger spatial resolution. Particularly, in the north part where herbaceous

385 dominates the vegetation layer, the higher correlation between VOD and *in situ* green biomass data indicates that
386 VOD is more robust to herbaceous species compositions, which is also supported by the less variation of the
387 scatter plots (the shade part of Fig. 4C) between VOD and woody cover. The water content in wood forms part
388 of the VOD base level and act as a bias for green biomass estimation that gradually increase from < 0.1 in the
389 north to < 0.3 in the south (Fig. 4A). The variation of this bias (water content in wood) should be limit in areas
390 with low woody cover. Yet, the influence of variation of this bias would make a difference in areas with high
391 woody cover, which should be one possible reason for the poor performance of VOD metrics on reflecting green
392 biomass dynamics in the south part (Fig. 5 and Table 1). Therefore, VOD is a potential proxy for the total
393 biomass yet the proportionality for water content with green and woody biomass needs to be corrected for.

394 Averaging the VOD/NDVI metrics and *in situ* biomass data over all the sites minimized the biases caused by
395 scale difference, hence we can draw implications from the performance of different season metrics (Table 2) on
396 the way to use VOD and NDVI for biomass estimation. For VOD, the good performance of October
397 observations corresponding to the period of maximum accumulation of biomass (when ground measurements
398 were collected) indicates that the water content in the total vegetation layer is highly correlated to the green
399 biomass. The reason why the annual sum performs better than the large integral may be that the sum includes
400 information of water content in wood during the dry season which may contribute to the foliage production in
401 October. The poorer performance of the VOD small integral may be caused by the missing information of water
402 content in wood that responsible for the base level of the VOD curve and plays an important role in the
403 photosynthetic process for producing biomass. For NDVI, the good performance of the small integral in
404 capturing biomass temporal dynamics were also documented for the Sahel by Fensholt et al. (2013) and Olsen et
405 al. (2015). A possible reason would be that the recurrent part of the vegetation layer forms the dominant part of
406 the net primary production (NPP) and that information from the green part of perennial vegetation (included in
407 annual sum and large integral) is influenced by varying atmospheric conditions and soil background during the
408 period of the dry season (approximately 9 months). The artifacts of GIMMS3g NDVI product in the dry season
409 during 2004–2011 (Horion et al. 2014) also have greater impacts on the performance of the annual sum and large
410 integral than the small integral. The NDVI annual max has been used as a proxy for the maximum vegetation

411 productivity (Evans and Geerken 2004; Fuller 1998; Jeyaseelan et al. 2007). However, in a study by Olsson et
412 al. (2005) a much more widespread greening of the Sahel was found when calculated from seasonal NDVI
413 integrals as compared to trend estimates calculated from the seasonal NDVI amplitude. This was explained by
414 the possible saturation of the NDVI signal, thereby rendering the NDVI seasonal amplitude less sensitive to
415 detection of changes in dryland areas. This is supported by the results presented here (Fig. 4C and Fig. 5)
416 showing that the saturation effect has an impact on biomass estimation for the greener parts of the Sahelian
417 drylands.

418 Vegetation long-term trend analysis based on different AHVRR NDVI products have been performed from
419 regional to global scales to assist discussions on land degradation trends in drylands in general and in the Sahel
420 in particular (Fensholt et al. 2012; Herrmann et al. 2014; Mbow et al. 2015; Olsson et al. 2005). However, the
421 quality of these NDVI products due to a series of sensor issues and the resulting greening/browning trends have
422 been questioned (Beck et al. 2011; de Beurs and Henebry 2004; Tian et al. 2015). The long-term VOD dataset
423 derived from passive microwave observations provides an important independent source to the NDVI based
424 approaches for land degradation assessment. The results shown in this study would benefit the future usage of
425 VOD data on vegetation trend analysis. The coarse spatial resolution of VOD impedes its applicability at the
426 local scale, but is of less concern for studies at regional, continental or global scales.

427 **6. Conclusion**

428 An improved understanding of the characteristics and responses of the satellite passive microwave
429 observation based VOD to vegetation variations is achieved by comparison with the well-studied GIMMS3g
430 NDVI and *in situ* measurements in the semi-arid Senegalese Sahel covering a gradient of mixtures of woody and
431 herbaceous vegetation lifeforms in drylands. VOD has proven to be an efficient proxy for green biomass of the
432 entire vegetation stratum (both woody foliage and herbaceous) and is a potential proxy for the total biomass as it
433 also sensitive to the water content in the standing wood mass. VOD shows an increased sensitivity to
434 information on the woody layer and is found to be less affected by saturation effect as compared to NDVI in the
435 greener parts of dryland areas. VOD also appears to be less sensitive to vegetation species composition in

monitoring dryland biomass production as compared to greenness measures derived from visible/near-infrared parts of the spectrum. It is concluded that the different sensitivity of VOD and NDVI to total water content and chlorophyll abundance respectively causes different seasonal metrics to be optimal for biomass monitoring amongst the two sensor systems. The integration of the greenness seasonality is most closely related to *in situ* measured biomass, while the VOD works equally well as a proxy for biomass when used as a "snapshot" in time (October, when the *in situ green* biomass was measured). Also the annual sum of VOD was found to perform well due to possible linkage between water content in the persistent part of the woody vegetation during dry season and foliage production at the end of growing season. Our results suggest that a complementary use of VOD and NDVI would allow for more complete monitoring of dryland vegetation resources. With the higher sensitivity of VOD to woody vegetation water content, the long-term VOD dataset would help to improve our understanding of woody cover/biomass variations in drylands which is currently a challenge for regional/large scale optical remote sensing. On the other hand seasonal metrics of NDVI is still well suited for monitoring of the herbaceous stratum and obviously the capabilities of doing so with high spatial resolution is of importance for many applications.

Acknowledgments

This research is partly funded by the China Scholarship Council (CSC, number 201306420005), the Danish Council for Independent Research (DFF) Sapere Aude programme under the project entitled "Earth Observation based Vegetation productivity and Land Degradation Trends in Global Drylands", and a Project Funded by the Priority Academic Program Development of Jiangsu Higher Education Institutions (PAPD). Martin Brandt is the recipient of the European Union's Horizon 2020 research and innovation programme under the Marie Sklodowska-Curie grant agreement (No. 656564). Yi Y. Liu is the recipient of an Australian Research Council Discovery Early Career Researcher Award (DECRA) Fellowship (No. DE140100200). Aleixandre Verger is the recipient of a Juan de la Cierva postdoctoral fellowship from the Spanish Ministry of Science and Innovation.

References

Achard, F., & Blasco, F. (1990). Analysis of vegetation seasonal evolution and mapping of forest cover in West Africa with the use of NOAA AVHRR HRPT data. *Photogrammetric Engineering & Remote Sensing, 56*, 1359-1365

Adeel, Z., Safriel, U., Niemeijer, D., White, R., de Kalbermatten, G., Glantz, M., Salem, B., Scholes, B., Niamir-Fuller, M., Ehui, S., & Yapi-Gnaore, V. (2005). *Ecosystems and human well-being: desertification synthesis. A Report of the Millennium Ecosystem Assessment*. Washington, DC: World Resources Institute

Ahearn, S.C., & de Rooy, C. (1996). Monitoring the effects of Dracunculiasis remediation on agricultural productivity using satellite data. *International Journal of Remote Sensing, 17*, 917-929

Ahlstrom, A., Raupach, M.R., Schurgers, G., Smith, B., Arneth, A., Jung, M., Reichstein, M., Canadell, J.G., Friedlingstein, P., Jain, A.K., Kato, E., Poulter, B., Sitch, S., Stocker, B.D., Viovy, N., Wang, Y.P., Wiltshire, A., Zaehle, S., & Zeng, N. (2015). The dominant role of semi-arid ecosystems in the trend and variability of the land CO2 sink. *Science, 348*, 895-899

Andela, N., Liu, Y.Y., van Dijk, A.I.J.M., de Jeu, R.A.M., & McVicar, T.R. (2013). Global changes in dryland vegetation dynamics (1988-2008) assessed by satellite remote sensing: comparing a new passive microwave vegetation density record with reflective greenness data. *Biogeosciences, 10*, 6657-6676

Beck, H.E., McVicar, T.R., van Dijk, A.I.J.M., Schellekens, J., de Jeu, R.A.M., & Bruijnzeel, L.A. (2011). Global evaluation of four AVHRR–NDVI data sets: Intercomparison and assessment against Landsat imagery. *Remote Sensing of Environment, 115*, 2547-2563

Becker, F., & Choudhury, B.J. (1988). Relative sensitivity of normalized difference vegetation Index (NDVI) and microwave polarization difference Index (MPDI) for vegetation and desertification monitoring. *Remote Sensing of Environment, 24*, 297-311

Brandt, M., Hiernaux, P., Tagesson, T., Verger, A., Rasmussen, K., Diouf, A.A., Mbow, C., Mougin, E., & Fensholt, R. (2015a). Woody plant cover estimation in drylands from Earth Observation based seasonal metrics. *Remote Sensing of Environment, Under Review*

Brandt, M., Hiernaux, P., Tagesson, T., Verger, A., Rasmussen, K., Diouf, A.A., Mbow, C., Mougin, E., & Fensholt, R. (2016). Woody plant cover estimation in drylands from Earth Observation based seasonal metrics. *Remote Sensing of Environment, 172*, 28-38

Brandt, M., Mbow, C., Diouf, A.A., Verger, A., Samimi, C., & Fensholt, R. (2015b). Ground- and satellite-based evidence of the biophysical mechanisms behind the greening Sahel. *Global Change Biology*, 1610-1620

Cao, C., Xiong, X., Wu, A., & Wu, X. (2008). Assessing the consistency of AVHRR and MODIS L1B reflectance for generating fundamental climate data records. *Journal of Geophysical Research-Atmospheres, 113*

Choudhury, B.J., & Tucker, C.J. (1987). Monitoring global vegetation using Nimbus-7 37 GHz Data Some empirical relations. *International Journal of Remote Sensing, 8*, 1085-1090

Choudhury, B.J., Tucker, C.J., Golus, R.E., & Newcomb, W.W. (1987). Monitoring vegetation using Nimbus-7 scanning multichannel microwave radiometer's data. *International Journal of Remote Sensing, 8*, 533-538

Cissé, M.I. (1980). The browse production of some trees of the Sahel: relationships between maximum foliage biomass and various physical parameters. *Browse in Africa* (pp. 205-210): ILCA Addis Ababa, Ethiopia

Dardel, C., Kergoat, L., Hiernaux, P., Mougin, E., Grippa, M., & Tucker, C.J. (2014). Re-greening Sahel: 30 years of remote sensing data and field observations (Mali, Niger). *Remote Sensing of Environment, 140*, 350-364

de Beurs, K.M., & Henebry, G.M. (2004). Trend Analysis of the Pathfinder AVHRR Land (PAL) NDVI Data for the Deserts of Central Asia. *Ieee Geoscience and Remote Sensing Letters, 1*, 282-286

de Jong, R., de Bruin, S., de Wit, A., Schaepman, M.E., & Dent, D.L. (2011). Analysis of monotonic greening and browning trends from global NDVI time-series. *Remote Sensing of Environment, 115*, 692-702

de Ridder, N., Stroosnijder, L., & Cisse, A.M. (1982). *Productivity of Sahelian rangelands : a study of the soils, the vegetations and the exploitation of that natural resource*. Wageningen: Agricultural University

Diallo, O., Diouf, A., Hanan, N.P., Ndiaye, A., & PrÉVost, Y. (1991). AVHRR monitoring of savanna primary production in Senegal, West Africa: 1987-1988. *International Journal of Remote Sensing, 12*, 1259-1279

Diouf, A., Brandt, M., Verger, A., Jarroudi, M., Djaby, B., Fensholt, R., Ndione, J., & Tychon, B. (2015). Fodder Biomass Monitoring in Sahelian Rangelands Using Phenological Metrics from FAPAR Time Series. *Remote Sensing, 7*, 9122

Diouf, A., & Lambin, E.F. (2001). Monitoring land-cover changes in semi-arid regions: remote sensing data and field observations in the Ferlo, Senegal. *Journal of Arid Environments, 48*, 129-148

Diouf, A., Sall, M., Wélé, A., & Dramé, M. (1998). Sampling method of primary production in the field (technical document). In (p. 9): Centre de Suivi Ecologique of Dakar

Evans, J., & Geerken, R. (2004). Discrimination between climate and human-induced dryland degradation. *Journal of Arid Environments, 57*, 535-554

Fensholt, R. (2004). Earth observation of vegetation status in the Sahelian and Sudanian West Africa: comparison of Terra MODIS and NOAA AVHRR satellite data. *International Journal of Remote Sensing, 25*, 1641-1659

Fensholt, R., Anyamba, A., Huber, S., Proud, S.R., Tucker, C.J., Small, J., Pak, E., Rasmussen, M.O., Sandholt, I., & Shisanya, C. (2011). Analysing the advantages of high temporal resolution geostationary MSG SEVIRI data compared to Polar Operational Environmental Satellite data for land surface monitoring in Africa. *International Journal of Applied Earth Observation and Geoinformation, 13*, 721-729

Fensholt, R., Anyamba, A., Stisen, S., Sandholt, I., Pak, E., & Small, J. (2007). Comparisons of Compositing Period Length for Vegetation Index Data from Polar-orbiting and Geostationary Satellites for the Cloud-prone Region of West Africa. *Photogrammetric Engineering & Remote Sensing, 73*, 297-309

Fensholt, R., Horion, S., Tagesson, T., Ehammer, A., Ivits, E., & Rasmussen, K. (2015). Global-scale mapping of changes in ecosystem functioning from earth observation-based trends in total and recurrent vegetation. *Global Ecology and Biogeography, 24*, 1003-1017

Fensholt, R., Huber, S., Proud, S.R., & Mbow, C. (2010). Detecting Canopy Water Status Using Shortwave Infrared Reflectance Data From Polar Orbiting and Geostationary Platforms. *Ieee Journal of Selected Topics in Applied Earth Observations and Remote Sensing, 3*, 271-285

Fensholt, R., Langanke, T., Rasmussen, K., Reenberg, A., Prince, S.D., Tucker, C., Scholes, R.J., Le, Q.B., Bondeau, A., Eastman, R., Epstein, H., Gaughan, A.E., Hellden, U., Mbow, C., Olsson, L., Paruelo, J., Schweitzer, C., Seaquist, J., & Wessels, K. (2012). Greenness in semi-arid areas across the globe 1981–2007 — an Earth Observing Satellite based analysis of trends and drivers. *Remote Sensing of Environment, 121*, 144-158

Fensholt, R., & Proud, S.R. (2012). Evaluation of Earth Observation based global long term vegetation trends — Comparing GIMMS and MODIS global NDVI time series. *Remote Sensing of Environment, 119*, 131-147

Fensholt, R., Rasmussen, K., Kaspersen, P., Huber, S., Horion, S., & Swinnen, E. (2013). Assessing Land Degradation/Recovery in the African Sahel from Long-Term Earth Observation Based Primary Productivity and Precipitation Relationships. *Remote Sensing, 5*, 664-686

Fensholt, R., Rasmussen, K., Nielsen, T.T., & Mbow, C. (2009). Evaluation of earth observation based long term vegetation trends — Intercomparing NDVI time series trend analysis consistency of Sahel from AVHRR GIMMS, Terra MODIS and SPOT VGT data. *Remote Sensing of Environment, 113*, 1886-1898

Fensholt, R., Sandholt, I., & Stisen, S. (2006). Evaluating MODIS, MERIS, and VEGETATION vegetation indices using in situ measurements in a semi-arid environment. *Ieee Transactions on Geoscience and Remote Sensing, 44*, 1174-1786

Fuller, D.O. (1998). Trends in NDVI time series and their relation to rangeland and crop production in Senegal, 1987-1993. *International Journal of Remote Sensing, 19*, 2013-2018

Gitelson, A.A., Kaufman, Y.J., & Merzlyak, M.N. (1996). Use of a green channel in remote sensing of global vegetation from EOS-MODIS. *Remote Sensing of Environment, 58*, 289-298

Goetz, S.J., Prince, S.D., Goward, S.N., Thawley, M.M., & Small, J. (1999). Satellite remote sensing of primary production: an improved production efficiency modeling approach. *Ecological Modelling, 122*, 239-255

Gonzalez, P., Tucker, C.J., & Sy, H. (2012). Tree density and species decline in the African Sahel attributable to climate. *Journal of Arid Environments, 78*, 55-64

Guan, K., Good, S.P., Caylor, K.K., Sato, H., Wood, E.F., & Li, H. (2014). Continental-scale impacts of intra-seasonal rainfall variability on simulated ecosystem responses in Africa. *Biogeosciences, 11*, 6939-6954

Herrmann, S.M., Sall, I., & Sy, O. (2014). People and pixels in the Sahel: a study linking coarse-resolution remote sensing observations to land users' perceptions of their changing environment in Senegal. *Ecology and Society, 19*

Hiernaux, P. (1980). Inventory of the browse potential of bushes, trees and shrubs in an area of the Sahel in Mali: method and initial results. *Browse in Africa*, 205

Hiernaux, P., Diarra, L., Trichon, V., Mougin, E., Soumaguel, N., & Baup, F. (2009). Woody plant population dynamics in response to climate changes from 1984 to 2006 in Sahel (Gourma, Mali). *Journal of Hydrology, S0022-1694(09)00135-8*, HYDROL 16508

Holben, B.N. (1986). Characteristics of maximum-value composite images from temporal AVHRR data. *International Journal of Remote Sensing, 7*, 1417-1434

Horion, S., Fensholt, R., Tagesson, T., & Ehammer, A. (2014). Using earth observation-based dry season NDVI trends for assessment of changes in tree cover in the Sahel. *International Journal of Remote Sensing, 35*, 2493-2515

Jackson, T.J., Cosh, M.H., Bindlish, R., Starks, P.J., Bosch, D.D., Seyfried, M., Goodrich, D.C., Moran, M.S., & Jinyang, D. (2010). Validation of Advanced Microwave Scanning Radiometer Soil Moisture Products. *Ieee Transactions on Geoscience and Remote Sensing, 48*, 4256-4272

Jackson, T.J., & Schmugge, T.J. (1991). Vegetation effects on the microwave emission of soils. *Remote Sensing of Environment, 36*, 203-212

Jeyaseelan, A.T., Roy, P.S., & Young, S.S. (2007). Persistent changes in NDVI between 1982 and 2003 over India using AVHRR GIMMS (Global Inventory Modeling and Mapping Studies) data. *International Journal of Remote Sensing, 28*, 4927-4946

Jones, M., Kimball, J., Small, E., & Larson, K. (2014). Comparing land surface phenology derived from satellite and GPS network microwave remote sensing. *International Journal of Biometeorology, 58*, 1305-1315

Jones, M.O., Jones, L.A., Kimball, J.S., & McDonald, K.C. (2011). Satellite passive microwave remote sensing for monitoring global land surface phenology. *Remote Sensing of Environment, 115*, 1102-1114

Jones, M.O., Kimball, J.S., & Jones, L.A. (2013). Satellite microwave detection of boreal forest recovery from the extreme 2004 wildfires in Alaska and Canada. *Global Change Biology, 19*, 3111-3122

Jones, M.O., Kimball, J.S., Jones, L.A., & McDonald, K.C. (2012). Satellite passive microwave detection of North America start of season. *Remote Sensing of Environment, 123*, 324-333

Jonsson, P., & Eklundh, L. (2002). Seasonality extraction by function fitting to time-series of satellite sensor data. *Ieee Transactions on Geoscience and Remote Sensing, 40*, 1824-1832

Jonsson, P., & Eklundh, L. (2004). TIMESAT - a program for analyzing time-series of satellite sensor data. *Computers & Geosciences, 30*, 833-845

Knapp, A.K., Fay, P.A., Blair, J.M., Collins, S.L., Smith, M.D., Carlisle, J.D., Harper, C.W., Danner, B.T., Lett, M.S., & McCarron, J.K. (2002). Rainfall Variability, Carbon Cycling, and Plant Species Diversity in a Mesic Grassland. *Science, 298*, 2202-2205

Le Houérou, H.N. (1980). The rangelands of the Sahel. *Journal of Range Management, 33*, 41-46

Liu, Y.Y., de Jeu, R.A.M., McCabe, M.F., Evans, J.P., & van Dijk, A.I.J.M. (2011a). Global long-term passive microwave satellite-based retrievals of vegetation optical depth. *Geophysical Research Letters, 38*

Liu, Y.Y., Evans, J.P., McCabe, M.F., de Jeu, R.A.M., van Dijk, A.I.J.M., Dolman, A.J., & Saizen, I. (2013a). Changing Climate and Overgrazing Are Decimating Mongolian Steppes. *Plos One, 8*, e57599

Liu, Y.Y., Parinussa, R.M., Dorigo, W.A., De Jeu, R.A.M., Wagner, W., van Dijk, A.I.J.M., McCabe, M.F., & Evans, J.P. (2011b). Developing an improved soil moisture dataset by blending passive and active microwave satellite-based retrievals. *Hydrology and Earth System Sciences, 15*, 425-436

Liu, Y.Y., van Dijk, A.I.J.M., de Jeu, R.A.M., Canadell, J.G., McCabe, M.F., Evans, J.P., & Wang, G. (2015). Recent reversal in loss of global terrestrial biomass. *Nature Climate Change, 5*, 470-474

Liu, Y.Y., van Dijk, A.I.J.M., McCabe, M.F., Evans, J.P., & de Jeu, R.A.M. (2013b). Global vegetation biomass change (1988–2008) and attribution to environmental and human drivers. *Global Ecology and Biogeography, 22*, 692-705

Los, S.O. (1998). Estimation of the ratio of sensor degradation between NOAA AVHRR channels 1 and 2 from monthly NDVI composites. *Ieee Transactions on Geoscience and Remote Sensing, 36*, 206-213

Mbow, C., Brandt, M., Ouedraogo, I., de Leeuw, J., & Marshall, M. (2015). What Four Decades of Earth Observation Tell Us about Land Degradation in the Sahel? *Remote Sensing, 7*, 4048

Mbow, C., Fensholt, R., Rasmussen, K., & Diop, D. (2013). Can vegetation productivity be derived from greenness in a semi-arid environment? Evidence from ground-based measurements. *Journal of Arid Environments, 97*, 56-65

Meesters, A.G.C.A., de Jeu, R.A.M., & Owe, M. (2005). Analytical derivation of the vegetation optical depth from the microwave polarization difference index. *Ieee Geoscience and Remote Sensing Letters, 2*, 121-123

Meroni, M., Rembold, F., Verstraete, M., Gommes, R., Schucknecht, A., & Beye, G. (2014). Investigating the Relationship between the Inter-Annual Variability of Satellite-Derived Vegetation Phenology and a Proxy of Biomass Production in the Sahel. *Remote Sensing, 6*, 5868

Milich, L., & Weiss, E. (2000). GAC NDVI images: Relationship to rainfall and potential evaporation in the grazing lands of The Gourma (northern Sahel) and in the croplands of the Niger-Nigeria border (southern Sahel). *International Journal of Remote Sensing, 21*, 261-280

Min, Q., & Lin, B. (2006). Remote sensing of evapotranspiration and carbon uptake at Harvard Forest. *Remote Sensing of Environment, 100*, 379-387

Mo, T., Choudhury, B.J., Schmugge, T.J., Wang, J.R., & Jackson, T.J. (1982). A model for microwave emission from vegetation-covered fields. *Journal of Geophysical Research: Oceans, 87*, 11229-11237

Mougin, E., Demarez, V., Diawara, M., Hiernaux, P., Soumaguel, N., & Berg, A. (2014). Estimation of LAI, fAPAR and fCover of Sahel rangelands (Gourma, Mali). *Agricultural and Forest Meteorology, 198–199*, 155-167

628 Mougin, E., Lo Seena, D., Rambal, S., Gaston, A., & Hiernaux, P. (1995). A regional Sahelian grassland model
629 to be coupled with multispectral satellite data. I: Model description and validation. *Remote Sensing of*
630 *Environment, 52*, 181-193

631 Myneni, R.B., & Hall, F.G. (1995). The interpretation of spectral vegetation indexes. *Ieee Transactions on*
632 *Geoscience and Remote Sensing, 33*, 481-486

633 Myneni, R.B., Keeling, C.D., Tucker, C.J., Asrar, G., & Nemani, R.R. (1997). Increased plant growth in the
634 northern high latitudes from 1981 to 1991. *Nature, 386*, 698-702

635 Nemani, R.R., Keeling, C.D., Hashimoto, H., Jolly, W.M., Piper, S.C., Tucker, C.J., Myneni, R.B., & Running,
636 S.W. (2003). Climate-driven increases in global terrestrial net primary production from 1982 to 1999. *Science,*
637 *300*, 1560-1563

638 Njoku, E.G., & Chan, S.K. (2006). Vegetation and surface roughness effects on AMSR-E land observations.
639 *Remote Sensing of Environment, 100*, 190-199

640 Novella, N.S., & Thiaw, W.M. (2013). African Rainfall Climatology Version 2 for Famine Early Warning
641 Systems. *Journal of Applied Meteorology and Climatology, 52*, 588-606

642 Olsen, J.L., Miehe, S., Ceccato, P., & Fensholt, R. (2015). Does EO NDVI seasonal metrics capture variations in
643 species composition and biomass due to grazing in semi-arid grassland savannas? *Biogeosciences, 12*, 4407-
644 4419

645 Olsson, L., Eklundh, L., & Ardö, J. (2005). A recent greening of the Sahel—trends, patterns and potential
646 causes. *Journal of Arid Environments, 63*, 556-566

647 Owe, M., de Jeu, R., & Holmes, T. (2008). Multisensor historical climatology of satellite-derived global land
648 surface moisture. *Journal of Geophysical Research-Earth Surface, 113*

649 Owe, M., de Jeu, R., & Walker, J. (2001). A methodology for surface soil moisture and vegetation optical depth
650 retrieval using the microwave polarization difference index. *Ieee Transactions on Geoscience and Remote*
651 *Sensing, 39*, 1643-1654

652 Pinzon, J., Brown, M.E., & Tucker, C.J. (2005). Satellite time series correction of orbital drift artifacts using
653 empirical mode decomposition. In N. Huang (Ed.), *Hilbert-Huang transform: introduction and applications* (pp.
654 167-186)

655 Pinzon, J., & Tucker, C. (2014). A non-stationary 1981–2012 AVHRR $NDVI3_g$ time series. *Remote Sensing, 6*,
656 6929-6960

657 Poulter, B., Frank, D., Ciais, P., Myneni, R.B., Andela, N., Bi, J., Broquet, G., Canadell, J.G., Chevallier, F.,
658 Liu, Y.Y., Running, S.W., Sitch, S., & van der Werf, G.R. (2014). Contribution of semi-arid ecosystems to
659 interannual variability of the global carbon cycle. *Nature, 509*, 600-603

660 Prince, S.D. (1991). Satellite remote sensing of primary production: comparison of results for Sahelian
661 grasslands 1981-1988. *International Journal of Remote Sensing, 12*, 1301-1311

662 Prince, S.D., & Goward, S.N. (1995). Global Primary Production: A Remote Sensing Approach. *Journal of*
663 *Biogeography, 22*, 815-835

664 Qian, C., Jiancheng, S., Jinyang, D., Tianjie, Z., & Chuan, X. (2015). An Approach for Monitoring Global
665 Vegetation Based on Multiangular Observations From SMOS. *Selected Topics in Applied Earth Observations*
666 *and Remote Sensing, IEEE Journal of, 8*, 604-616

667 Rietkerk, M., Ketner, P., Stroosnijder, L., & Prins, H.H.T. (1996). Sahelian rangeland development; a
668 catastrophe? *Journal of Range Mangagement, 49*, 512-519

669 Sellers, P.J. (1985). Canopy reflectance, photosynthesis and transpiration. *International Journal of Remote*
670 *Sensing, 6*, 1335-1372

Shi, J., Jackson, T., Tao, J., Du, J., Bindlish, R., Lu, L., & Chen, K.S. (2008). Microwave vegetation indices for short vegetation covers from satellite passive microwave sensor AMSR-E. *Remote Sensing of Environment, 112*, 4285-4300

Solano, R., Didan, K., Jacobson, A., & Huete, A. (2010). MODIS Vegetation Index User's Guide (MOD13 Series). In

Spiekermann, R., Brandt, M., & Samimi, C. (2015). Woody vegetation and land cover changes in the Sahel of Mali (1967–2011). *International Journal of Applied Earth Observation and Geoinformation, 34*, 113-121

Tagesson, T., Fensholt, R., Guiro, I., Rasmussen, M.O., Huber, S., Mbow, C., Garcia, M., Horion, S., Sandholt, I., Holm-Rasmussen, B., Göttsche, F.M., Ridler, M.-E., Olén, N., Lundegard Olsen, J., Ehammer, A., Madsen, M., Olesen, F.S., & Ardö, J. (2015). Ecosystem properties of semiarid savanna grassland in West Africa and its relationship with environmental variability. *Global Change Biology, 21*, 250-264

Tagesson, T., Mastepanov, M., Molder, M., Tamstorf, M.P., Eklundh, L., Smith, B., Sigsgaard, C., Lund, M., Ekberg, A., Falk, J.M., Friborg, T., Christensen, T.R., & Strom, L. (2013). Modelling of growing season methane fluxes in a high-Arctic wet tundra ecosystem 1997-2010 using in situ and high-resolution satellite data. *Tellus Series B-Chemical and Physical Meteorology, 65*

Tian, F., Fensholt, R., Verbesselt, J., Grogan, K., Horion, S., & Wang, Y. (2015). Evaluating temporal consistency of long-term global NDVI datasets for trend analysis. *Remote Sensing of Environment, 163*, 326-340

Tian, F., Wang, Y., Fensholt, R., Wang, K., Zhang, L., & Huang, Y. (2013). Mapping and Evaluation of NDVI Trends from Synthetic Time Series Obtained by Blending Landsat and MODIS Data around a Coalfield on the Loess Plateau. *Remote Sensing, 5*, 4255-4279

Tucker, C.J. (1979). Red and photographic infrared linear combinations for monitoring vegetation. *Remote Sensing of Environment, 8*, 127-150

Tucker, C.J., Pinzon, J.E., Brown, M.E., Slayback, D.A., Pak, E.W., Mahoney, R., Vermote, E.F., & El Saleous, N. (2005). An extended AVHRR 8-km NDVI dataset compatible with MODIS and SPOT vegetation NDVI data. *International Journal of Remote Sensing, 26*, 4485-4498

Tucker, C.J., & Sellers, P.J. (1986). Satellite remote sensing of primary production. *International Journal of Remote Sensing, 7*, 1395-1416

Tucker, C.J., Vanpraet, C., Boerwinkel, E., & Gaston, A. (1983). Satellite remote sensing of total dry matter production in the Senegalese Sahel. *Remote Sensing of Environment, 13*, 461-474

Vermote, E., & Kaufman, Y.J. (1995). Absolute calibration of AVHRR visible and near-infrared channels using ocean and cloud views. *International Journal of Remote Sensing, 16*, 2317-2340

Wessels, K.J., Prince, S.D., Zambatis, N., MacFadyen, S., Frost, P.E., & Van Zyl, D. (2006). Relationship between herbaceous biomass and 1-km^2 Advanced Very High Resolution Radiometer (AVHRR) NDVI in Kruger National Park, South Africa. *International Journal of Remote Sensing, 27*, 951-973

Wezel, A., & Schlecht, E. (2004). Inter-annual variation of species composition of fallow vegetation in semi-arid Niger. *Journal of Arid Environments, 56*, 265-282

Wu, X.Q., Sullivan, J.T., & Heidinger, A.K. (2010). Operational calibration of the Advanced Very High Resolution Radiometer (AVHRR) visible and near-infrared channels. *Canadian Journal of Remote Sensing, 36*, 602-616

Zeng, J., Li, Z., Chen, Q., Bi, H., Qiu, J., & Zou, P. (2015). Evaluation of remotely sensed and reanalysis soil moisture products over the Tibetan Plateau using in-situ observations. *Remote Sensing of Environment, 163*, 91-110

Supplementary

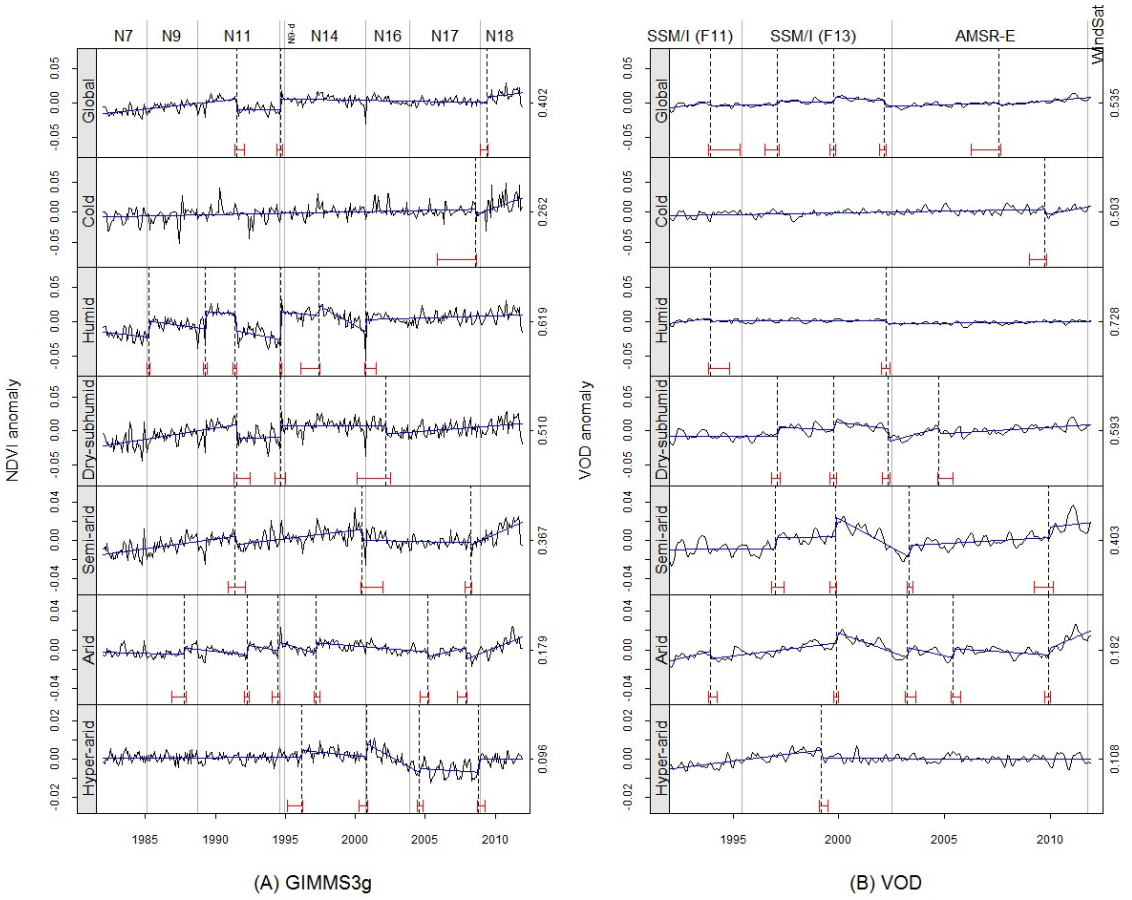

Fig. S1. Evaluation of temporal consistency for (A) GIMMS3g NDVI and (B) VOD by examining global and humidity zone averaged anomaly series. The ranges of y-axis are set in line with Fig. 4 in Tian et al. (2015) and the values on the right-hand of y-axis are mean of each original NDVI/VOD series. Results of GIMMS3g are shown for the time period used in this study (1992–2011).

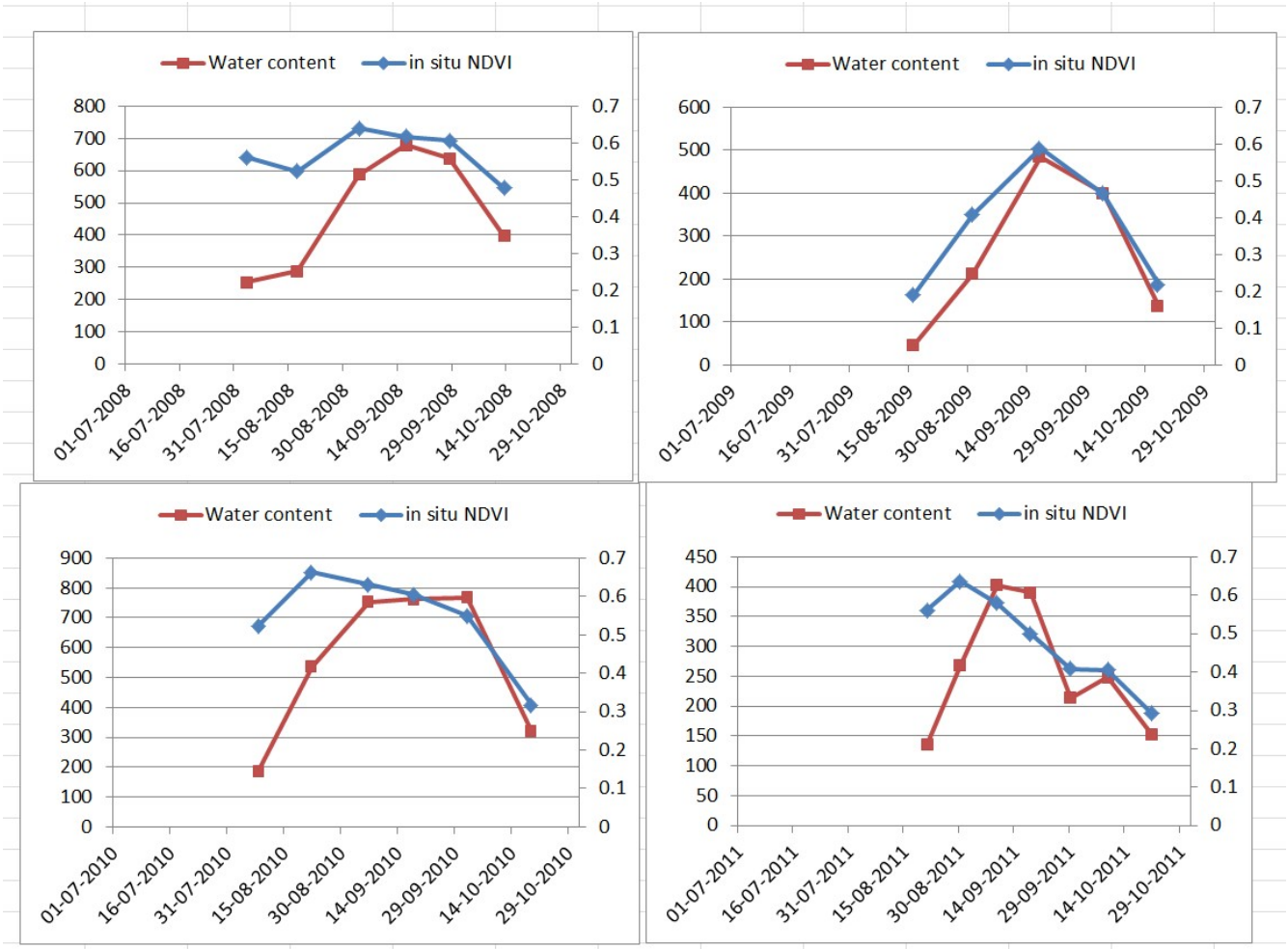

720

721 **Fig. S2.** The water content and in situ NDVI collected during 2008-2011 at Dahra field site in Senegal. Please refer to

722 (Tagesson et al. 2015) and (Mbow et al. 2013) for detailed information.